Hindawi
Journal of Chemistry
Volume 2019, Article ID 3568185, 8 pages
https://doi.org/10.1155/2019/3568185

Research Article

A Novel Approach for Fabricating $LaMnO_3$ Thin Films Using Combined Microwave Combustion and Pulsed Electron Deposition Techniques

Thi Ha Tran,[1] Thi Trung Anh Tang,[2] Nguyen Hai Pham,[2] Thanh Cong Bach,[2] Cong Doanh Sai,[2] Quang Hoa Nguyen,[2] Van Vu Le,[2] Hoang Nam Nguyen,[2] Quoc Khoa Doan,[3] Trong Tam Nguyen,[4] Viet Bau Le,[5] Khac Hieu Ho,[6] and Viet Tuyen Nguyen[2]

[1]*Hanoi University of Mining and Geology, Duc Thang, Tu Liem, Hanoi, Vietnam*
[2]*VNU University of Science, Vietnam National University, 334 Nguyen Trai, Thanh Xuan, Hanoi, Vietnam*
[3]*Quang Tri Teacher Training College, Quang Tri, Vietnam*
[4]*Department of Physics, Faculty of Basic–Fundamental Sciences, Vietnam Maritime University, 484 Lach Tray, Le Chan, Hai Phong, Vietnam*
[5]*Hong Duc University, 565 Quang Trung, Dong Ve, Thanh Hoa, Vietnam*
[6]*Duy Tan University, 03 Quang Trung, Danang, Vietnam*

Correspondence should be addressed to Cong Doanh Sai; saidoanh@hus.edu.vn and Viet Tuyen Nguyen; nguyenviettuyen@hus.edu.vn

Received 28 November 2018; Accepted 5 February 2019; Published 4 March 2019

Guest Editor: Ajit Kumar Sharma

$LaMnO_3$ (LMO) nanopowder was synthesized by the microwave combustion method using glycine and nitrate salts of La and Mn as precursors. The as-prepared LMO powder was pressed at high pressure and annealed at 1000°C for 8 hours to make a target for thin film deposition. The structural and elemental analysis was obtained by X-ray diffraction (XRD) and energy dispersive X-ray spectroscopy (EDS). Thin films of LMO were fabricated using pulsed electron deposition (PED) at room temperature. The effects of discharge voltage and oxygen/argon flux ratio on the produced thin films were studied. The study shows that stoichiometry and structure of the target was preserved well in the thin films prepared with a discharge voltage from 14 to 15 kV, while the oxygen/nitrogen flux ratio did not show a clear effect on the quality of thin films.

1. Introduction

Recently, semiconductor magnetic nanomaterials have received much awareness than that of their same bulk materials, due to their size and surface effects, which exhibit unique properties such as photoluminescence, magneto-optical, electrochemical, and photocatalytic activity [1–13]. These unique properties of nanomaterials in turn help to solve a lot of urgent problems related to exhaustion of fossil fuels and environment pollution. In this aspect, production and application of clean fuels based on nanomaterials become more and more critical for the development of human society [14–17]. In particular, solid oxide fuel cells (SOFCs) have been extensively studied and attracted much attention as a promising way to generate electricity at high efficiency and low cost [18–20]. For such applications, the cathode material must satisfy several criteria such as good electrical conductivity, high porosity to allow gas diffusion, thermal expansion coefficient matching well with that of the solid electrolyte, and chemical stability at a high temperature

[21–23]. Most of the requirements listed above are satisfied by $LaMnO_3$ perovskites, making it one of the most suitable materials for cathode in SOFCs [24].

Among many effective methods developed to produce nanopowders, microwave-assisted synthesis was first developed in 1985 and has quickly become a major area of study. Since microwave radiations were discovered, these have been widely utilized for synthetic chemistry in order to activate chemical reactions more rapidly and homogeneously [25–29]. Moreover, a self-combustion reaction assisted with microwave is extremely suitable for preparation of perovskite nanomaterials due to notable advantages such as simple and convenient experimental set-up, extremely time, and energy saving, as well as offering homogeneous product [30–32]. These advantages result from a thorough blending among the constituents in an aqueous media under microwave irradiation. Furthermore, an exothermic redox reaction between the fuel and an oxidizer provides a great amount of heat which is necessary for the formation of the perovskite phase [33, 34].

In general, thin films can be manufactured by a variety of methods such as sputtering, thermal evaporation, and molecular-beam epitaxy [35–37]. Pulsed electron deposition (PED) is also a physical thin film deposition technique offering many advantages such as high film homogeneity and low cost. However, this method seems to be not explored for preparation of perovskite thin films even though it is convenient to transfer the target stoichiometry to the deposited films by PED [38].

In this paper, $LaMnO_3$ (LMO) nanopowder was prepared by microwave combustion where glycine was used as a fuel in a combustion reaction with nitrate salts of lanthanum and manganese. The as-prepared LMO powder was pressed and annealed at 1000°C for 8 hours to make a target for thin film deposition. The fabrication of LMO thin films by PED was investigated in details.

2. Experiment

$LaMnO_3$ nanopowder was prepared by the microwave combustion method. Analytical grade La_2O_3 (99.99%), $Mn(NO_3)_2{\cdot}4H_2O$ (99%), and glycine NH_2CH_2COOH (99%) were used as the starting materials. Stoichiometric amount of La_2O_3 was dissolved in HNO_3 to obtain $La(NO_3)_3$ solution. Then, $La(NO_3)_3$ and $Mn(NO_3)_2$ solutions in water at molar ratio of 1 : 1 were mixed well before dropwise addition of glycine.

We first prepared a set of samples with different molar ratios of glycine to the metal ion ($F = 2.5$, 3, 3.5, 4, and 4.5) to study the effect of fuel on the nanoproduct. After heating on a hot plate at 150°C, the light pink solution evolved into a colorless transparent one and then viscous brown gel. Gel was stored in a glass container covered with an open lid and then quickly transferred to a microwave oven. After a few seconds, the viscous gel bubbled up and autoignited to produce brown fine powder.

The LMO powder was milled, pressed, and annealed at 1000°C for 8 hours to make a target for fabrication of the thin film by pulsed electron deposition system PEBS-20 from Neocera, Inc. All the $LaMnO_3$ films were deposited on silicon substrates with the repetition rate of pulses maintained at 5 Hz, pulse width of 100 ns, and 20 000 pulses.

Two sets of thin film samples were prepared to study the effect of discharge voltage (LMO-1) and O_2/N_2 flux ratio (LMO-2). The deposition of the LMO-1 films was carried out at room temperature and at five discharge voltages: 11, 12, 13, 14, and 15 kV. The N_2 gas and O_2 gas were introduced at a pressure of 9×10^{-3} Torr for enhancing the electron beam and stabilizing the beam propagation to the target with a gas flux of 10 sccm and 15 sccm for oxygen and nitrogen, respectively. LMO-2 films were fabricated at 15 kV with various flux ratios of oxygen and nitrogen: 0 : 25; 5 : 20; 10 : 15; 20 : 5; and 25 : 0 sccm. During the deposition process, the pressure was maintained by balancing between the rate of the turbopump and the flow rate of oxygen and nitrogen gas introduced into the chamber. The as-deposited thin films were annealed at 400, 600, and 800°C for 2 h.

The crystallinity of the thin films was characterized by the X-ray diffraction system (Siemens D5005, Bruker, Germany) with Cu $K_{\alpha 1}$ ($\lambda = 0.154056$ nm) radiation. The morphology of the product was investigated by a scanning electron microscope (Nova Nano SEM 450). The composition of the samples was verified by energy dispersive X-ray (EDX) spectrometry (Oxford Isis 300) integrated into the JEOL-JSM 5410 scanning electron microscope.

3. Results and Discussion

Figure 1 shows XRD patterns of $LaMnO_3$ nanoparticles prepared by the microwave irradiation method when using glycine as fuel in the combustion reaction with the glycine-nitrate molar ratio (G/N) ($F = 2.5$, 3, 3.5, 4, and 4.5).

The sample prepared with $F = 2.5$ is amorphous because the released energy is not enough for formation of the perovskite phase. With $F = 3$, 3.5, 4, and 4.5, the $LaMnO_3$ perovskite phase has formed. Sharp and intense XRD peaks of the samples with $F = 3$ suggested that crystal quality of those samples is better. The combustion reaction with a higher value of F liberated more heat. However, gas generated during the reaction can bring out heat from the reaction chamber and reduced the heat used for synthesis of the perovskite material [39]. Heat generated by the reaction might be reduced too much and resulted in an amorphous state of samples with F greater than 4. XRD patterns indicate that $LaMnO_3$ nanoparticles, prepared with $F = 3$; 3.5; and 4, crystallized in a hexagonal structure. Lattice parameters and crystalline size of the samples prepared with different ratios of F are shown in Table 1.

XRD analysis of the $LaMnO_3$ nanoparticles prepared by combustion assisted with microwave irradiation also shows the presence of both $LaMnO_3$ and La_2CO_5. La_2CO_5 is an unwanted phase due to the unavoidable reaction of metal ions with organic precursors.

A pure perovskite is necessary for making cathode of good performance fuel cell. Therefore, such secondary phases need to be removed. As an unsolvable material, La_2CO_5 cannot be washed away using water, so the nanopowder was annealed at 1000°C to convert the remaining

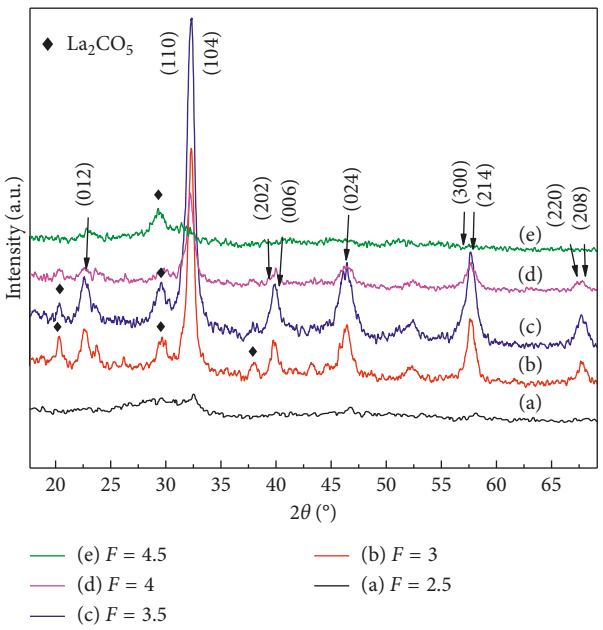

Figure 1: XRD patterns of $LaMnO_3$ nanoparticles with $F = 2.5$, 3, 3.5, 4, and 4.5.

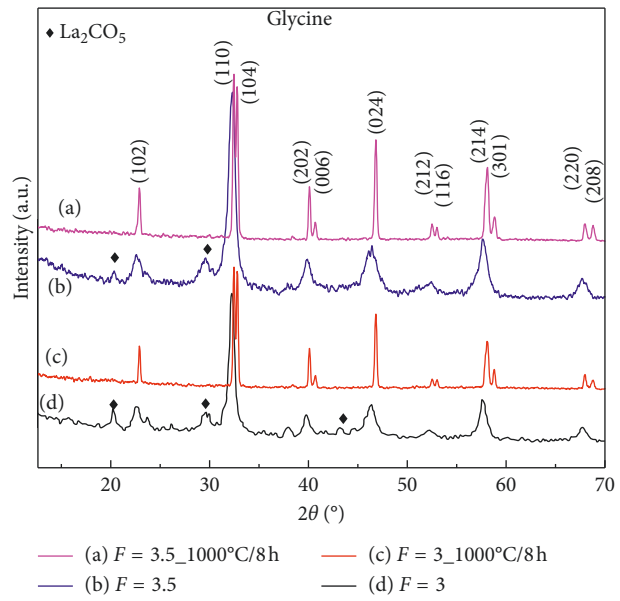

Figure 2: XRD patterns of $LaMnO_3$ samples with $F = 3$ and 3.5 before and after annealing at 1000°C in 8 h.

Table 1: The lattice parameters and crystallite size of the $LaMnO_3$ samples with different ratios of glycine/nitrate molar ($F = 3$, 3.5, and 4).

Sample	a (Å)	b (Å)	c (Å)	$\overline{d}$ (nm)	Volume of unit cell (Å^3)
$F = 3$	5.54	5.54	13.46	14.1	357.66
$F = 3.5$	5.54	5.54	13.47	10.2	357.62
$F = 4$	5.55	5.55	13.45	9.9	358.98

La_2CO_5 into $LaMnO_3$. Figure 2 shows the XRD patterns of $LaMnO_3$ samples with a molar ratio of glycine to metal ion of 3 and 3.5 before and after annealing at 1000°C in 8 h. After annealing, no peak related to La_2CO_5 can be seen in the XRD pattern. The result implies the purity of the final nanopowder. Sharper and stronger diffraction peaks show that crystalline sizes of the $LaMnO_3$ powder increase clearly after annealing, as expected due to the crystal growth during the annealing process at a high temperature. It should be also noted that, after annealing, a clear peak shift to a higher angle was observed. The reason for lattice expansion in the sample should be taken into account. One possible explanation for lattice expansion in the sample before annealing is small particles size. In other words, in nanomaterials of poor structural order, defect might be introduced at a high concentration, which results in an internal stress in the lattice due to the presence of large La^{3+} at interstitial sites in the lattice. The internal stress is responsible for the lattice expansion, as observed for as-prepared nanopowder samples. The corresponding decrease of the lattice parameter is shown in Table 2.

However, the results show that annealing the samples at 1000°C does not result in transition of the phase structure. Such peak shift to a higher angle, combining with the disappearance of some peaks in the XRD pattern, can be an indication of a phase transition. The change in the lattice parameter suggests that annealing phase transition from hexagonal to other structures can occur at a higher temperature or in longer time. However, this is not being mentioned in this paper but would be reported in another study.

The energy dispersive X-ray spectra (Figure 3) of the $LaMnO_3$ nanopowder with $F = 3$ before and after annealing at 1000°C in 8 hours only show the peaks of La, O, and Mn. This result indicates that samples are clean and pure. $LaMnO_3$ nanopowder prepared with a molar ratio of glycine/nitrate ($F = 3$) was used to make a target because the results showed that better crystallinity was achieved for this sample. The as-prepared LMO powder was remilled, pressed at high pressure, and annealed at 1000°C for 8 hours to make a target. The structure and phase purity of the LMO target was examined by XRD measurements, as shown in Figure 4. The XRD patterns reveal that the structure of the LMO target is still hexagonal. The LMO target showed peaks corresponding to reflection from (102), (110), (104), (202), (204), (212), (214), and (220) planes, where (110) and (104) peaks have the strongest intensity clearly demonstrating the preferred crystal growth during the annealing process.

Even though the LMO target can be fabricated by the normal solid-state reaction method from oxides precursors, using nanopowder of LMO to make the target help in reducing the treating temperature to 1000°C, the target prepared by the solid-state reaction normally required a much higher annealing temperature (1300–1400°C) and longer time (12–24 h).

Figure 5 shows XRD patterns of the $LaMnO_3$ thin films deposited at 15 kV before and after annealing at different temperatures. It can be seen that the as-deposited films and films annealed at 400°C and 600°C were amorphous because no diffraction peak is observed. As annealing temperature is

Table 2: The lattice parameter of the $LaMnO_3$ samples with different ratios of glycine/nitrate molar ($F = 3$ and 3.5) before and after annealing at 1000°C for 8 h.

Sample	a (Å)	b (Å)	c (Å)	Volume of unit cell (Å^3)
$F = 3$	5.54	5.54	13.46	357.66
$F = 3$ at 1000°C	5.51	5.51	13.29	349.43
$F = 3.5$	5.54	5.54	13.47	357.62
$F = 3.5$ at 1000°C	5.51	5.51	13.28	351.17

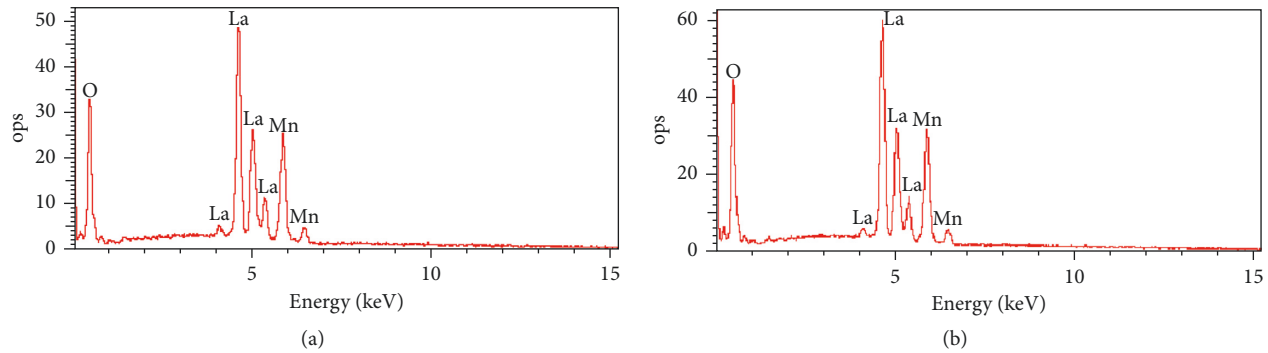

Figure 3: EDS spectra of the $LaMnO_3$ nanopowder with $F = 3$ (a) before and (b) after annealing at 1000°C.

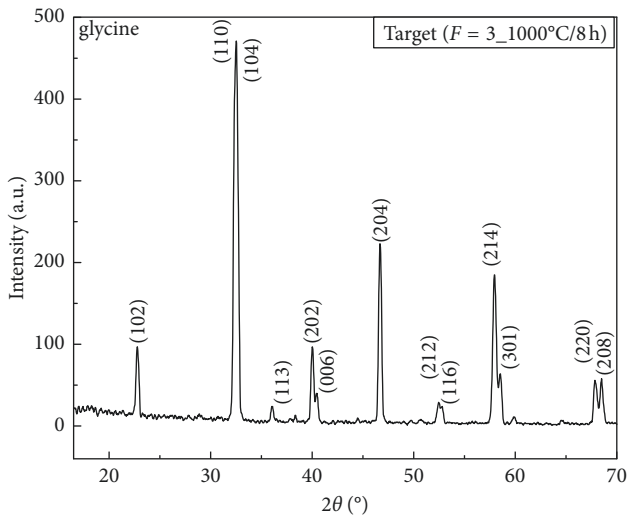

Figure 4: XRD pattern of the $LaMnO_3$ target made of $LaMnO_3$ nanoparticles prepared by self-combustion assisted with microwave irradiation.

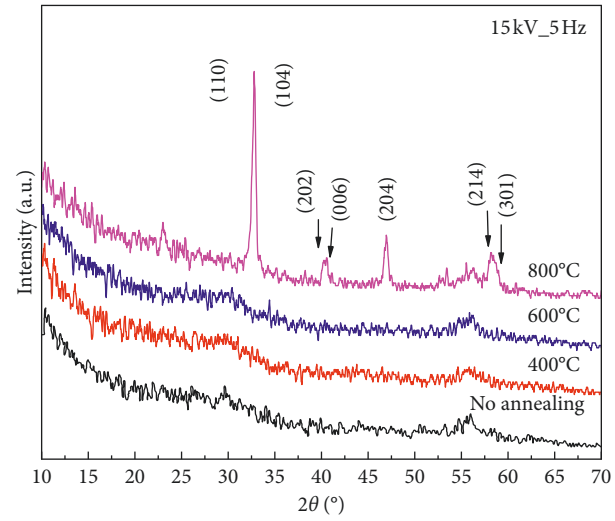

Figure 5: XRD patterns of the $LaMnO_3$ thin films deposited before and after annealing at 400°C, 600°C, and 800°C with a discharging voltage of 15 kV.

raised up to 800°C, the thin film is crystallined in the hexagonal structure.

Figure 6 shows SEM images of LMO thin films deposited at 15 kV before and after annealing at different temperatures.

SEM images of thin films deposited at 15 kV show that the particle size distribution is quite uniform and post-annealing does not change the morphology of the produced thin films. The film is crack free both before and after being annealed. SEM images also reveal that the films have uniform particulates which are uniformly distributed on the surface.

XRD analysis (Figure 7) shows that all thin films are amorphous for all discharge voltage. Postannealing at a temperature higher than 800°C is required to obtain crystalline films. However, transition from the amorphous to hexagonal structure occurs only in films deposited at 14 and 15 kV. Other films prepared at voltage lower than 14 kV remains in the amorphous state despite postannealing.

The diffraction peaks were higher at 15 kV which is the maximum voltage available for the used PED system. The above results can be understood that discharge voltage is a critical factor determining the growth of thin films by PED. Voltage higher than 14 kV is required to preserve the

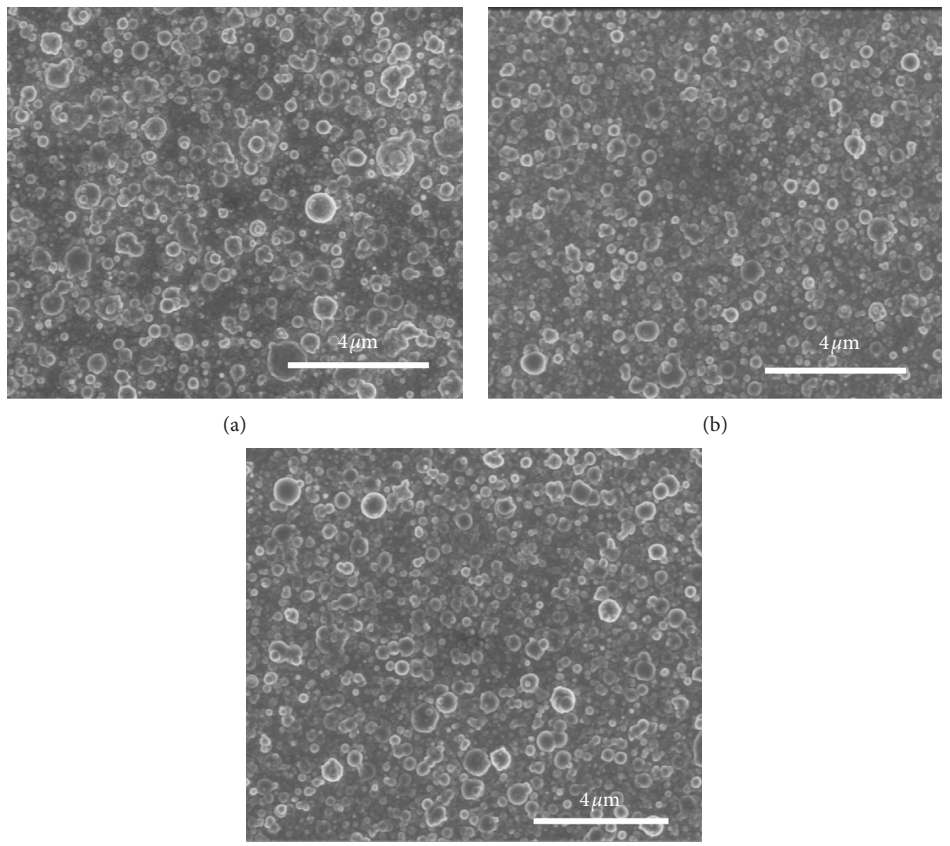

Figure 6: SEM images of LMO thin films deposition at 15 kV after annealing at different temperatures (a) as the deposited film: (b) 400°C; (c) 800°C.

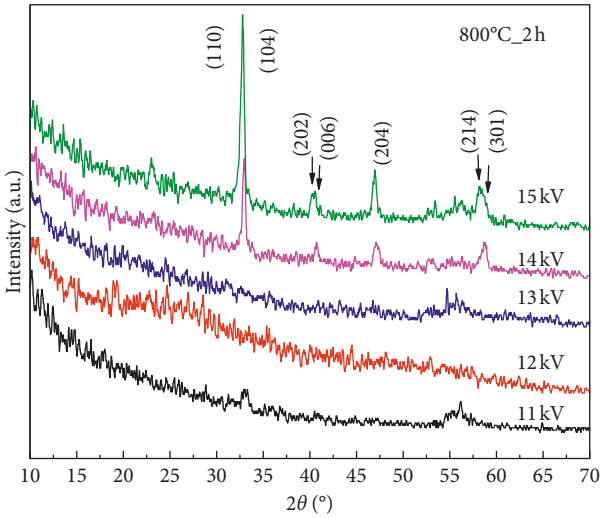

Figure 7: XRD patterns of $LaMnO_3$ thin films deposited at 11, 12, 13, 14, and 15 kV after annealing at 800°C for 2 h.

stoichiometry composition of the target to the thin films. However, the energy transferred by the electron beam is not enough for the atom to arrange on the substrate in a crystalline structure. Hence, postannealing is necessary to activate the crystallization of the thin films. Lattice parameters of the films prepared at 14 and 15 kV after annealing are shown in Table 3.

In vacuum deposition techniques, gas ambient may also have a great influence on the structure and morphology of the thin films [40]. We also studied the effect of the N_2/O_2 flux ratio on the LMO thin film prepared by pulse electron deposition. Figure 8 shows XRD patterns of the $LaMnO_3$ thin films deposited at 15 kV and 5 Hz with different ratios of N_2/O_2 flux (25 : 0, 20 : 5, 10 : 15, and 0 : 25 sccm).

It is clear that the films after postannealing are well crystallined at all different ratios of N_2/O_2 flux. The highest intensity was achieved for film grown at N_2/O_2 flux (10 : 15 sccm), indicating that partial pressure of oxygen also has a slight effect on the structure of the thin films.

Figure 9 shows SEM images of the LMO-2 films, which were prepared at a different oxygen partial pressure. While the sample prepared in pure nitrogen ambient possesses fine particulates, the samples prepared in oxygen show more particulates. This could be due to the fragmentation of the oxide particulates in the plasma region at higher oxygen partial pressures [41].

4. Conclusion

$LaMnO_3$ nanopowder was successfully synthesized using combustion assisted with microwave irradiation approach.

Table 3: The lattice parameters of the $LaMnO_3$ thin films deposited at 14 and 15 kV after annealing at 800°C for 2 h.

Sample	Lattice structure	a (Å)	b (Å)	c (Å)	Volume of unit cell (Å^3)
15 kV at 800°C	Hexagonal	5.46	5.46	13.44	358.03
14 kV at 800°C	Hexagonal	5.49	5.49	13.26	346.24

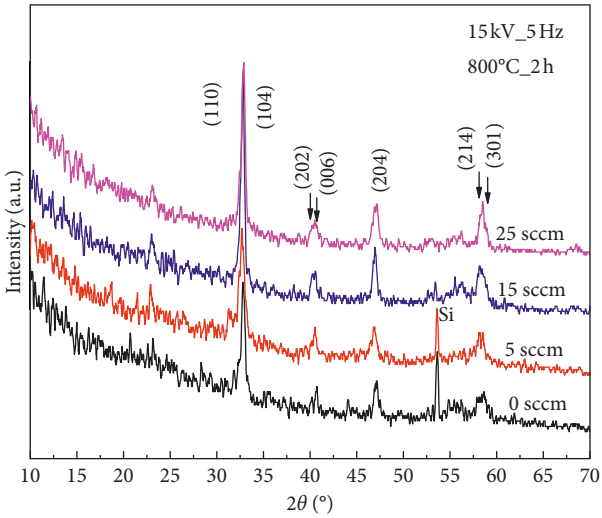

Figure 8: XRD patterns of the $LaMnO_3$ thin films prepared with different O_2 flux at 0, 5, 15, and 25 sccm after annealing at 800°C for 2 h.

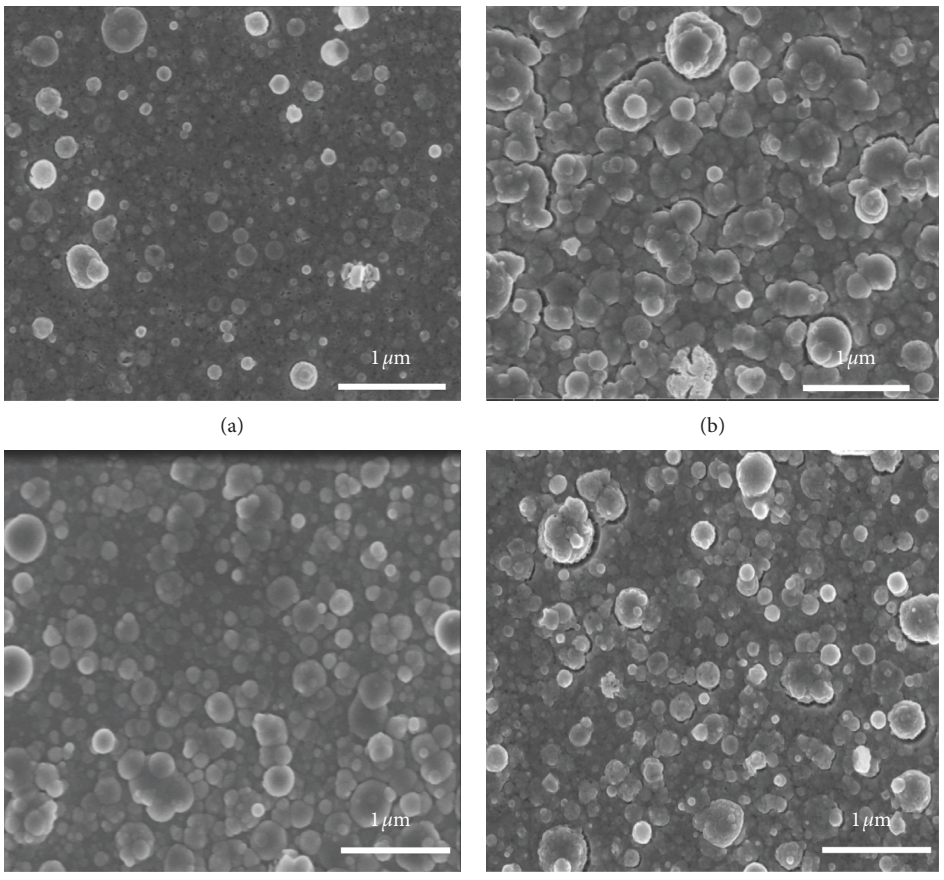

Figure 9: SEM image of $LaMnO_3$ thin films with different O_2 flux at (a) 0, (b) 5, (c) 15, and (d) 25 sccm after annealing at 800°C for 2 h.

Using nanopowder helps to lower the temperature of heat treatment of the target. Detailed investigation of $LaMnO_3$ thin films preparation shows that discharge voltage is a critical parameter for film deposition by PED. The obtained films were amorphous but could be converted into the crystalline phase after annealing at relatively a low temperature of 800°C. Suitable ratio of oxygen/nitrogen flux also contributes to better crystal quality of the thin films. The results demonstrate the potential of using PED as a tool for fabrication of perovskite thin films of high quality for various applications in electronic fields.

Data Availability

All data used to support the findings of this study are available from the corresponding author upon request.

Conflicts of Interest

The authors declare that they have no conflicts of interest.

Acknowledgments

The authors would like to thank Faculty of Physics, VNU University of Science, for allowing them to use the equipment. This research was funded by the Vietnam National University (VNU), Hanoi, under project number QG.17.11.

References

[1] M. Maria Lumina Sonia, S. Anand, S. Blessi, S. Pauline, and A. Manikandan, "Effect of surfactants (PVB/EDTA/CTAB) assisted sol-gel synthesis on structural, magnetic and dielectric properties of $NiFe_2O_4$ nanoparticles," *Ceramics International*, vol. 44, no. 18, pp. 22068–22079, 2018.

[2] M. M. L. Sonia, S. Anand, V. M. Vinosel, M. A. Janifer, S. Pauline, and A. Manikandan, "Effect of lattice strain on structure, morphology and magneto-dielectric properties of spinel $NiGd_xFe_{2-x}O_4$ ferrite nano-crystallites synthesized by sol-gel route," *Journal of Magnetism and Magnetic Materials*, vol. 466, pp. 238–251, 2018.

[3] S. Asiri, M. Sertkol, H. Güngüneş et al., "The temperature effect on magnetic properties of $NiFe_2O_4$ nanoparticles," *Journal of Inorganic and Organometallic Polymers and Materials*, vol. 28, no. 4, pp. 1587–1597, 2018.

[4] A. G. Abraham, A. Manikandan, E. Manikandan, S. K. Jaganathan, A. Baykal, and P. S. Renganathan, "Enhanced opto-magneto properties of $Ni_xMg_{1-x}Fe_2O_4$ ($0.0 < x < 1.0$) Ferrites nano-catalysts," *Journal of Nanoelectronics and Optoelectronics*, vol. 12, no. 12, pp. 1326–1333, 2017.

[5] A. Manikandan, M. Durka, M. Amutha Selvi, and S. Arul Antony, "Sesamum indicum plant extracted microwave combustion synthesis and opto-magnetic properties of spinel $Mn_xCo_{1-x}Al_2O_4$ nano-catalysts," *Journal of Nanoscience and Nanotechnology*, vol. 16, no. 1, pp. 448–456, 2016.

[6] H. H. Mai, V. T. Pham, V. T. Nguyen, C. D. Sai, C. H. Hoang, and T. B. Nguyen, "Non-enzymatic fluorescent biosensor for glucose sensing based on ZnO nanorods," *Journal of Electronic Materials*, vol. 46, no. 6, pp. 3714–3719, 2017.

[7] P. V. Thanh, H. Hanh Mai, N. V. Tuyen, S. C. Doanh, and N. C. Viet, "Zinc oxide nanorods grown on printed circuit board for extended-gate Field-effect transistor pH sensor," *Journal of Electronic Materials*, vol. 46, pp. 3732–3737, 2017.

[8] T. H. Tran and V. T. Nguyen, "Phase transition of Cu_2O to CuO nanocrystals by selective laser heating," *Materials Science in Semiconductor Processing*, vol. 46, pp. 6–9, 2016.

[9] T.-D. Pham and B. K. Lee, "Novel capture and photocatalytic conversion of CO_2 into solar fuels by metals co-doped TiO_2 deposited on PU under visible light," *Applied Catalysis A: General*, vol. 529, pp. 40–48, 2017.

[10] T.-D. Pham and B.-K. Lee, "Novel integrated approach of adsorption and photo-oxidation using Ag-TiO_2/PU for bioaerosol removal under visible light," *Chemical Engineering Journal*, vol. 275, pp. 357–365, 2015.

[11] T. D. Pham, B. K. Lee, M. V. Nguyen, and C. H. Lee, "Germicide Feasibility of TiO," *Advanced Materials Research*, vol. 518–523, pp. 864–868, 2012.

[12] T. D. Pham and B. K. Lee, "Novel integrated approach of adsorption and photo-oxidation using Ag–TiO_2/PU for bioaerosol removal under visible light," *Chemical Engineering Journal*, vol. 275, pp. 357–365, 275.

[13] T.-D. Pham and B.-K. Lee, "Photocatalytic comparison of Cu- and Ag-doped TiO_2/GF for bioaerosol disinfection under visible light," *Journal of Solid State Chemistry*, vol. 232, pp. 256–263, 2015.

[14] E. Hema, A. Manikandan, P. Karthika, M. Durka, S. A. Antony, and B. R. Venkatraman, "Magneto-optical properties of reusable spinel Ni," *Journal of Nanoscience and Nanotechnology*, vol. 16, no. 7, pp. 7325–7336, 2016.

[15] S. Suguna, S. Shankar, Saravana Kumar Jaganathan, and A. Manikandan, "Novel synthesis of spinel $Mn_xCo_{1-x}Al_2O_4$ (x = 0.0 to 1.0) nanocatalysts: effect of Mn^{2+} doping on structural, morphological, and opto-magnetic properties," *Journal of Superconductivity and Novel Magnetism*, vol. 30, no. 3, pp. 691–699, 2017.

[16] V. T. Nguyen, D. Nam, M. Gansukh et al., "Influence of sulfate residue on Cu_2ZnSnS_4 thin films prepared by direct solution method," *Solar Energy Materials and Solar Cells*, vol. 136, pp. 113–119, 2015.

[17] N. T. T. Truc, N. T. Hanh, M. V. Nguyen et al., "Novel direct Z-scheme $Cu_2V_2O_7$/g-C_3N_4 for visible light photocatalytic conversion of CO_2 into valuable fuels," *Applied Surface Science*, vol. 457, pp. 968–974, 2018.

[18] N. Mahato, A. Banerjee, A. Gupta, S. Omar, and K. Balani, "Progress in material selection for solid oxide fuel cell technology: a review," *Progress in Materials Science*, vol. 72, pp. 141–337, 2015.

[19] W. Wang, C. Su, Y. Wu, R. Ran, and Z. Shao, "Progress in solid oxide fuel cells with nickel-based Anodes operating on methane and related fuels," *Chemical Reviews*, vol. 113, no. 10, pp. 8104–8151, 2013.

[20] N. Minh, J. Mizusaki, and S. C. Singhal, "Advances in solid oxide fuel cells: review of progress through three decades of the international symposia on solid oxide fuel cells," *ECS Transactions*, vol. 78, no. 3, pp. 63–73, 2017.

[21] Y. Choi, E. C. Brown, S. M. Haile, and W. Jung, "Electrochemically modified, robust solid oxide fuel cell anode for direct-hydrocarbon utilization," *Nano Energy*, vol. 23, pp. 161–171, 2016.

[22] C. Yang, J. Li, Y. Lin, J. Liu, F. Chen, and M. Liu, "In situ fabrication of CoFe alloy nanoparticles structured $(Pr_{0.4}Sr_{0.6})_3(Fe_{0.85}Nb_{0.15})_2O_7$ ceramic anode for direct hydrocarbon solid oxide fuel cells," *Nano Energy*, vol. 11, pp. 704–710, 2015.

[23] V. A. Sadykov, V. S. Muzykantov, N. F. Yeremeev et al., "Solid oxide fuel cell cathodes: importance of chemical composition and morphology," *Catalysis for Sustainable Energy*, vol. 2, no. 1, pp. 57–70, 2015.

[24] C. Sun, R. Hui, and J. Roller, "Cathode materials for solid oxide fuel cells: a review," *Journal of Solid State Electrochemistry*, vol. 14, no. 7, pp. 1125–1144, 2010.

[25] T. Mistumori, K. Sasaki, K. Yano, R. Fujihara, and M. Yoshinaga, "Effects of microwave irradiation heating in the homogeneous precipitation method using the reductant generated by hydrolysis of urea in an autoclave under high pressure," *Journal of the Ceramic Society of Japan*, vol. 123, no. 5, pp. 359–362, 2015.

[26] T. T. Ha, T. D. Canh, and N. V. Tuyen, "A quick process for synthesis of ZnO nanoparticles with the aid of microwave irradiation," *ISRN Nanotechnology*, vol. 2013, Article ID 497873, 7 pages, 2013, 2013.

[27] N. V. Tuyen, T. D. Canh, N. N. Long, N. X. Nghia, B. N. Q. Trinh, and Z. Shen, "Synthesis of undoped and M-doped Zno (M = Co, Mn) nanopowder in water using microwave irradiation,"vol. 187, pp. 012020(1)–012020(8).

[28] T. D. Canh, N. V. Tuyen, and N. N. Long, "Influence of solvents on the growth of zinc oxide nanoparticles fabricated by microwave irradiation," *VNU Journal of Science: Mathematics—Physics*, vol. 25, pp. 71–76, 2009.

[29] N. V. Tuyen, N. N. Long, and T. D. Canh, "Synthesis and characteristics of single-crystal Ni-doped ZnO nanorods prepared by a microwave irradiation method," *e-Journal of Surface Science and Nanotechnology*, vol. 9, pp. 472–476, 2011.

[30] E. Hema, A. Manikandan, P. Karthika, S. A. Antony, and B. R. Venkatraman, "A novel synthesis of Zn^{2+}-doped $CoFe_2O_4$ spinel nanoparticles: structural, morphological, opto-magnetic and catalytic properties," *Journal of Superconductivity and Novel Magnetism*, vol. 28, no. 8, pp. 2539–2552, 2015.

[31] A. Manikandan, M. Durka, and S. A. Antony, "A novel synthesis, structural, morphological, and opto-magnetic characterizations of magnetically separable spinel $Co_x Mn_{1-x} Fe_2O_4$ ($0 \leq x \leq 1$) nano-catalysts," *Journal of Superconductivity and Novel Magnetism*, vol. 27, no. 12, pp. 2841–2857, 2014.

[32] T. H. Tran, T. C. Bach, N. H. Pham et al., "Phase transition of $LaMnO_3$ nanoparticles prepared by microwave assisted combustion method," *Materials Science in Semiconductor Processing*, vol. 89, pp. 121–125, 2019.

[33] A. Manikandan, R. Sridhar, S. Arul Antony, and S. Ramakrishna, "A simple aloe vera plant-extracted microwave and conventional combustion synthesis: morphological, optical, magnetic and catalytic properties of $CoFe_2O_4$ nanostructures," *Journal of Molecular Structure*, vol. 1076, pp. 188–200, 2014.

[34] M. Nüchter, B. Ondruschka, W. Bonrath, and A. Gum, "Microwave assisted synthesis—a critical technology overview," *Green Chemistry*, vol. 6, no. 3, pp. 128–141, 2004.

[35] L. M. Quynh, N. T. Tien, P. V. Thanh et al., "Optical and electrical responses of magnetron-sputtered amorphous Nb-doped TiO_2 thin films annealed at low temperature," *Physica B: Condensed Matter*, vol. 532, pp. 200–203, 2018.

[36] L. T. Dang, T. H. Dang, T. T. T. Nguyen et al., "Thermoelectric micro-refrigerator based on bismuth/Antimony telluride," *Journal of Electronic Materials*, vol. 46, no. 6, pp. 3660–3666, 2017.

[37] T. Ginley, Y. Wang, and S. Law, "Topological insulator film growth by molecular beam epitaxy: a review," *Crystals*, vol. 6, no. 11, p. 154, 2016.

[38] N. D. Sang, P. H. Quang, and D. Q. Ngoc, "Pulsed electron deposition (PED) - a novel tool for growth of thin films," *Communications in Physics*, vol. 22, no. 1, pp. 65–73, 2012.

[39] X. Pingbo, Z. Weiping, Y. Kuo, J. Long, Z. Weiwei, and X. Shangda, "Size-controllable gly–nitrate low temperature combustion synthesis (LCS) of nanocrystalline $La_{1-x}Sr_xMnO_3$," *Journal of Alloys and Compounds*, vol. 311, no. 1, pp. 90–92, 2000.

[40] C. S. Ma, S. K. Hau, K. H. Wong, P. W. Chan, and C. L. Choy, "The role of ambient gas scattering effect and lead oxide formation in pulsed laser deposition of lead-zirconate-titanate thin films," *Applied Physics Letters*, vol. 69, no. 14, pp. 2030–2032, 1996.

[41] K. Muthukkumaran, P. Kuppusami, R. Kesavamoorthy et al., "Microstructural studies of bulk and thin film GDC," *Ionics*, vol. 14, no. 2, pp. 165–171, 2008.